Molecular Therapy
Nucleic Acids
Original Article

Improved Cancer Targeting by Multimerizing Aptamers on Nanoscaffolds

Marjan Omer,[1,3,4] Veronica Liv Andersen,[1,3,4] Jesper Sejrup Nielsen,[1,3] Jesper Wengel,[2] and Jørgen Kjems[1,3]

[1]Interdisciplinary Nanoscience Center (iNANO), Aarhus University, Gustav Wieds Vej 14, 8000 Aarhus C, Denmark; [2]Biomolecular Nanoscale Engineering Center (BioNEC), Department of Physics, Chemistry and Pharmacy, University of Southern Denmark, Campusvej 55, 5230 Odense M, Denmark; [3]Center for Cellular Signal Patterns (CellPAT), Aarhus University, Gustav Wieds Vej 14, 8000 Aarhus C, Denmark

Aptamers are short single-stranded oligonucleotides selected to bind with high affinity and specificity to a target. In contrast to antibodies, aptamers can be produced in large-scale *in vitro* systems without the need for any biological agents, making them highly attractive as targeting ligands for bioimaging and drug delivery. For *in vivo* applications it is often desirable to multimerize the aptamers in order to increase their binding strength and overall specificity. Additional functionalities, such as imaging and therapeutic agents, as well as pharmacokinetic modifiers, need to be attached in a stoichiometric fashion. Herein, we present a robust method for assembly of up to three aptamers and a fluorophore in a single well-defined nanostructure. The process is entirely modular and can be applied to any aptamer requiring only a single reactive "click handle." Multimerization of two aptamers, A9g and GL21.T, previously shown to target cancer cells, led to a strong increase in cell uptake. A similar effect was observed for the prostate-specific membrane antigen (PSMA)-targeting A9g aptamer in mice where multivalent aptamer binding led to increased tumor specificity. Altogether, this method provides a platform for multimerization of aptamers with advantages in terms of combinatorial screening capacity and multifunctional design of nanomedicine.

INTRODUCTION

Bioimaging of diseases and delivery of precision medicine depend on the specific recognition of biomarkers to guide the process. A vital component is the development of suitable targeting ligands capable of selectively recognizing these biomarkers with high specificity.[1] The most successful example of this is humanized monoclonal antibodies (mAbs) specifically designed to recognize surface-bound disease biomarkers. However, due to the bulky nature of mAbs and the high development cost of antibody-based therapeutics, it is important to explore alternatives.

Aptamers make up an attractive class of targeting ligands. These are short DNA or RNA oligonucleotides, typically ~20–80 nucleotides (nt) long, selected for their ability to bind to a target molecule or a particular cell type.[2] Several therapeutically relevant aptamers have been selected and characterized *in vitro* and *in vivo*, including aptamers for vascular disorders, eye disease, and cancer.[3] Aptamers targeting cancer are particularly common, and a number of both DNA and RNA aptamers are currently in preclinical development.[4] These include aptamers that bind to the clinically relevant biomarker, prostate-specific membrane antigen (PSMA), a type II integral transmembrane glycoprotein with *N*-acetyl-L-aspartyl-L-glutamate peptidase activity that is significantly overexpressed on the surface of certain prostate cancer cells.[5]

Despite significant progress, the clinical translation of aptamers has been remarkably slow, and several prime candidates have failed during the early stages of clinical development. A particular problem appears to be poor efficacy *in vivo*, possibly due to low bioavailability and/or specificity.

In order to address these issues, many researchers have looked to antibodies for clues on how to improve the *in vivo* performance of aptamers. The most striking difference between antibodies and aptamers is that aptamers lack the increase in binding strength that arises from bitopic recognition. A simple solution would therefore be to assemble constructs displaying multivalent aptamers. Indeed, several such structures have been described in the literature. For example, bivalent variants of the 4-1BB and OX40 RNA aptamers were designed for cancer immunotherapy. Both aptamers bind to immune co-stimulatory receptors on T lymphocytes. The 4-1BB aptamer was dimerized by hybridization via a 21-nt 3′ overhang engineered on each aptamer to fit the distance requirement of the two receptor interactions.[6] In contrast, a biotinylated OX40 aptamer was assembled via non-covalent association with streptavidin.[7] This latter approach was also used to multimerize two biotinylated PSMA aptamers and two similarly modified small interfering RNAs (siRNAs).[8]

Although these studies demonstrate a modest increase in aptamer binding affinity, using streptavidin as a vehicle does not allow full control of ligand stoichiometry, especially when combining aptamers with different functionalities. Furthermore, clinical trial

Received 16 June 2020; accepted 10 October 2020;
https://doi.org/10.1016/j.omtn.2020.10.013.

[4]These authors contributed equally to this work.

Correspondence: Jørgen Kjems, Interdisciplinary Nanoscience Center (iNANO), Aarhus University, Gustav Wieds Vej 14, 8000 Aarhus C, Denmark.
E-mail: jk@mbg.au.dk

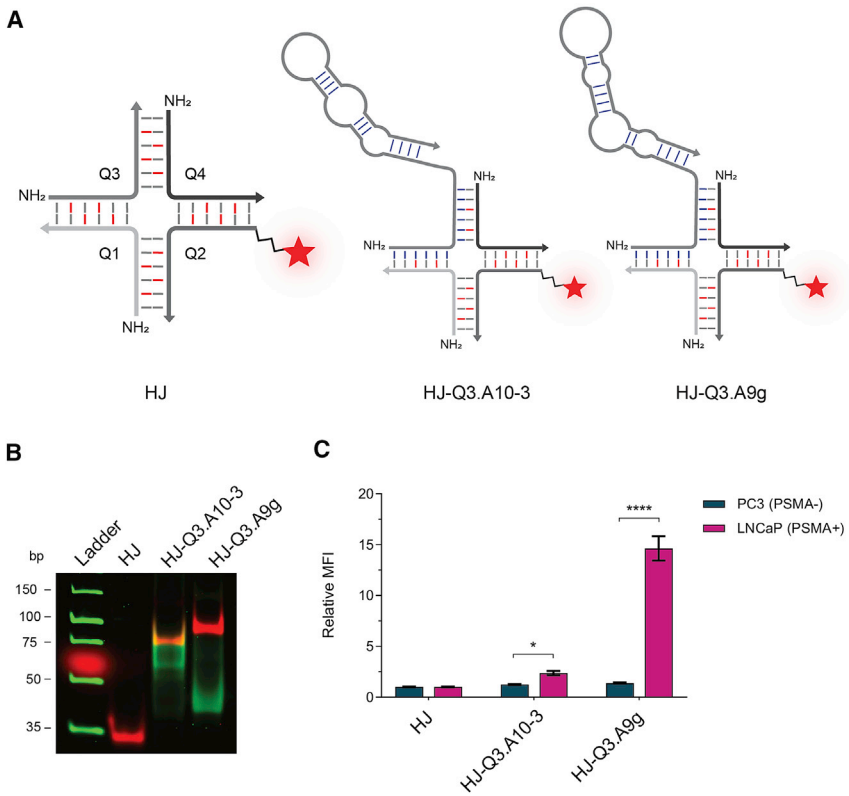

Figure 1. Functionalization of the HJ Scaffold with *In Vitro*-Transcribed Anti-PSMA Aptamers

(A) Schematics of A10-3- and A9g-functionalized HJ constructs (HJ-Q3.A10-3 and the HJ-Q3.A9g). Bases attached to LNA are shown in red, 2′-OMe in gray, and 2′-F/RNA in dark blue (see Figure S1 for nucleotide identities). Arrows indicate the 3′ ends. (B) A 12% native PAGE gel showing the assembly of a HJ, HJ-Q3.A10-3, and HJ-Q3.A9g. All three HJs have a Cy5 fluorophore (red) on the Q2 strand for detection by gel electrophoresis and in flow cytometry. Green shows SYBR Gold nucleic acid stain. The size marker is an ultra-low-range DNA ladder. The size marker xylene cyanol in the DNA ladder appears as a red spot from the Cy5 scan. (C) Uptake of HJ-Q3.A10-3 and the HJ-Q3.A9g (50 nM) in LNCaP/PC3$^-$ cells, analyzed by flow cytometry. The bars represent the quantified fluorescence from three biological replicates normalized to the free HJ. Uptake of both HJ-Q3.A10-3 and the HJ-Q3.A9g was significantly higher than for free HJs and only occurred in PSMA-positive cells. Statistical analysis was performed by one-way ANOVA followed by a Tukey's post hoc test. Error bars represent mean ± SD. *$p < 0.05$, ****$p < 0.0001$. MFI, median fluorescence intensity.

reports have shown that bacterial streptavidin induces undesirable immune responses and is therefore not suitable for therapeutic purposes.[9]

Recently, several groups have used DNA or RNA origami as a platform to multimerize aptamers. Owing to the principles of Watson-Crick base pairing, the spatial distance and stoichiometry of aptamers in such constructs can be precisely designed to improve aptamer binding. In one study, two thrombin-binding aptamers were incorporated into different RNA origami designs at different positions.[10] The greatest anticoagulant activity was observed when the two thrombin aptamers were in close proximity, in contrast to thrombin aptamers alone. While this strategy has certain advantages, the stability of such large DNA and RNA structures in biological systems may pose a concern, as these are susceptible to opsonization by the mononuclear phagocyte system as well as endonuclease and exonuclease activity in serum.[11]

Another promising approach has been to use nanoparticles to display a large number of aptamers;[12] however, nanoparticles suffer from biocompatibility issues, including uncontrolled liver retention, passive retention, as well as contamination from their synthesis.[13] As a result, there is an unmet need to establish a clinically safe and *in vivo*-stable scaffold for multimerizing aptamers in a stoichiometrically controlled fashion in combination with other types of targeting ligands, imaging tracers, and payloads.

We have recently developed a modular platform system termed the Holliday junction (HJ), which is capable of combining up to four different functionalities in a single, well-defined structure.[14] The HJ consists of four 12-nt-long, chemically modified nucleic acid modules with a chemical handle on each 5′ end, allowing simple click chemistry-based bioconjugation. This 3- to 4-nm large scaffold is highly stable *in vivo*, pharmacokinetically tunable, and can be targeted to specific organs using small-molecule ligands.[14]

In this study, we extend the use of the HJ to study the effect of aptamer multimerization for tumor targeting. By using simple copper-free click chemistry, we conjugated one to three aptamers covalently to the chemically modified HJ and demonstrated an increased homing to study the effect on targeting cancer cells *in vitro* and tumors *in vivo*.

RESULTS

Functionalization of the HJ with *In Vitro*-Transcribed Anti-PSMA Aptamers

The locked nucleic acid (LNA)-based HJ scaffold[14] was used as a platform for attachment and multimerization of aptamers. It consists of four 12-nt oligonucleotides (Q1, Q2, Q3, and Q4) containing a mixture of 2′-*O*-methyl (2′-OMe) and LNA nucleotides (indicated in gray and red, respectively, in Figure 1A).

As an initial strategy we replaced the Q3 arm with an extended version of the well-described PSMA-targeting aptamers A9g (43 nt)[15,16] and A10-3 (39 nt),[17] both of which have been shown to bind specifically to PSMA-expressing cells. The A10-3 aptamer was particularly interesting since it had been shown to facilitate internalization of an siRNA when hybridized to a 21-nt single-stranded extension,[18,19] indicating

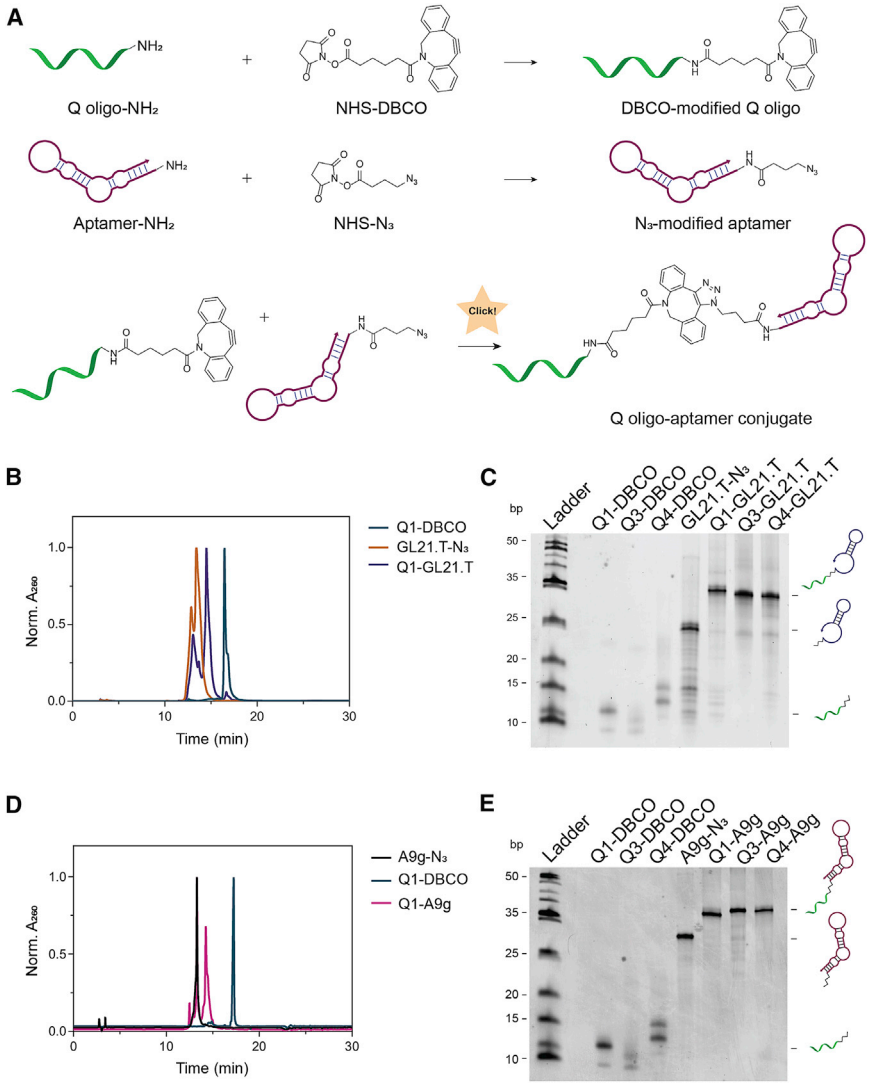

Figure 2. Covalent Conjugation of HJs with Synthetic Aptamers

(A) Reaction scheme for functionalization. The aptamer strands were reacted with NHS-azide bifunctional linkers, and the Q-oligonucleotides were labeled with NHS-DBCO linkers. After purification, the two strands were conjugated by copper-free click chemistry. (B) HPLC chromatogram of Q1-DBCO, GL21.T-N_3, and the Q1-GL21.T conjugate. (C) A 12% denaturing PAGE showing the products of the purified click reaction of Q1, Q3, and Q4 with GL21.T. (D) Elution profiles of Q1-DBCO, A9g-N_3, and the Q1-GL21.T conjugate. (E) Products of click reactions with Q1, Q3, Q4, and A9g analyzed on a 12% denaturing PAGE gel. The size marker in both gels is an ultra-low-range DNA ladder.

that A10-3 could be annealed to a nucleic acid scaffold without interfering with the binding activity of this aptamer.

Both aptamers were produced as *in vitro* transcripts with 5′ extensions mimicking the Q3 arm of the HJ (Figures 1A and S1). The aptamers were gel-purified and subsequently assembled with the Cy5-labeled Q2 and the remaining Q1 and Q4 arms of the HJ.

HJs assembled efficiently with both Q3.A10-3 and Q3.A9g replacing the Q3 arm. However, due to the absence of LNA-stabilized bases, it was found that an excess of both Q3.A10-3 and Q3.A9g was required to efficiently assemble the HJs; therefore, some residual aptamer transcripts were observed (Figure 1B). To test the targeting ability of the aptamer-presenting HJs, PSMA-positive prostate cancer cells (LNCaP) and PSMA-negative cells ($PC3^-$) were incubated with Cy5-labeled HJ-Q3.A10-3 and the HJ-Q3.A9g and analyzed by flow cytometry for cell association (Figure 1C). Both aptamers retained their binding capabilities when attached to the HJ scaffold based on the observation that both constructs bound significantly better to LNCaP cells compared to control HJ. Moreover, this effect was receptor-dependent, as the cell association in $PC3^-$ cells was not significantly different from the naked HJ. From these results the A9g aptamer appears to be the most potent targeting agent in accordance with previous reports.[15,16]

Covalent Conjugation of Aptamers

While hybridization of *in vitro*-transcribed strands was sufficient to attach a single aptamer to the HJ scaffold, such a strategy is not feasible for the assembly of multiple aptamers. To retain the LNA in all four strands, we devised a chemical conjugation strategy to create multivalent aptamer constructs.

Based on the results of the initial cell-association studies, we chose not to proceed with the A10-3 aptamer, as this did not appear to bind particularly well to PSMA-positive cells under these conditions. In order to address the flexibility of our approach, we included another unrelated aptamer, the 34-nt-long 2′-fluoro (2′-F) pyrimidine-modified aptamer GL21.T, which is a truncated version of the 92-mer GL21 aptamer reported to specifically bind the malignant human glioblastoma cell line U87MG.[20,21] The GL21.T aptamer was originally shown to bind with high affinity to the membrane-bound receptor tyrosine kinase (RTK) AXL.[21]

The GL21.T and A9g aptamers were chemically synthesized with a 5′-amino functional group and subsequently covalently conjugated to Q1, Q3, and Q4 oligonucleotides in a two-step copper-free click reaction, which is described in detail in Materials and Methods (Figure 2A). The Q oligonucleotide-aptamer conjugates were then purified by reverse-phase high-performance liquid chromatography (RP-HPLC), resulting in essentially pure products (Figures 2B–2E).

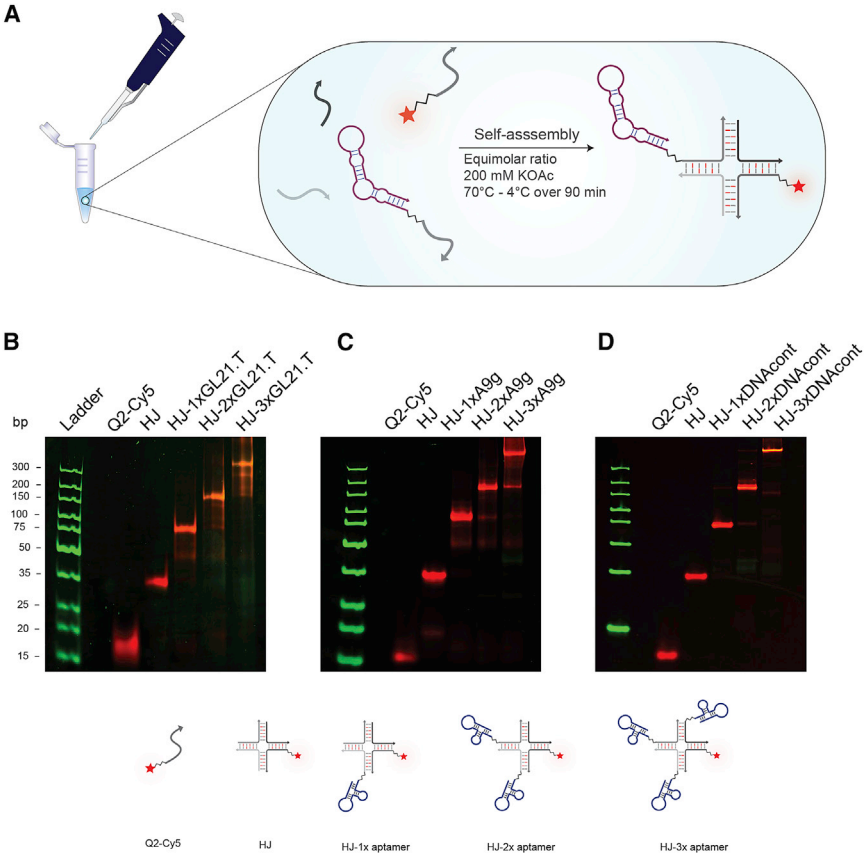

Figure 3. Assembly of Multimeric Aptamers on the HJ Platform

(A) Schematic illustration of the self-assembly process of aptamer-functionalized HJ. (B–D) Assembly of HJs with one to three copies of GL21.T (B), A9g (C), or DNAcont (D) aptamers with Cy5-labeled (red) Q2 for detection. Green signal is the SYBR Gold scan. The size marker in all gels is an ultra-low-range DNA ladder.

HJs were assembled with either purified GL21.T or A9g conjugates in one to three copies in equimolar amounts together with the remaining Q oligonucleotides. The Q2 oligonucleotide was labeled with Cy5 in all constructs to allow detection. All combinations of the HJs self-assembled with very high efficacy (>90%), thus eliminating the need for post-assembly purification (Figure 3).

Cell Targeting of Multimeric Aptamers

The membrane-bound RTK AXL is expressed on several different cancer cells, including the lung cancer cell line A549 but not the breast cancer cell line MCF-7.[21] To test the binding activity of the GL21.T-functionalized HJs, we incubated HJ alone or HJs carrying one, two, or three aptamers on Q1, Q3, and Q4 with the AXL-positive cell line A549 and two AXL-negative cell lines, MCF-7 and KB, and used flow cytometry to analyze specific binding efficiency. The results showed a significant increase in A549 cell uptake that correlated with the number of aptamers attached to the HJ (3-, 8-, and 11-fold increase with one, two, and three copies of GL21.T, respectively; Figures 4A and 4C).

To our surprise, an almost identical uptake was observed in the negative control MCF-7 cells while no appreciable uptake was detected in the KB cells. This uptake pattern was confirmed by confocal microscopy (Figure S2). These results are in marked contrast to the observation by Cerchia et al.,[21] who found that the GL21.T aptamer did not associate with MCF-7 cells. The unexpected result led us to investigate the AXL expression profile in all three cell lines by flow cytometry analysis (Figure S3). Using an AXL-specific antibody, flow cytometry showed that AXL was highly expressed in both A549 and KB cells, but absent in MCF-7 cells. We conclude that GL21.T is unlikely to recognize the AXL receptor and decided not to pursue further experiments using GL21.T.

The A9g-functionalized HJs were similarly tested for their ability to mediate binding and internalization in PSMA-positive ($PC3^+$ and LNCaP) and PSMA-negative ($PC3^-$) cells following the approach of Dassie et al.[16] We treated PSMA-positive and PSMA-negative cells with HJ alone or conjugated to one, two, or three A9g aptamers with Cy5-labeled Q2 and analyzed the cell association by flow cytometry (Figure 5A). Both PSMA-positive cell lines showed markedly increased uptake of A9g-conjugated HJ compared to the naked HJ. Importantly, there appears to be a clear avidity effect, most strongly observed between one to two copies of A9g (8-, 28-, and 42-fold increase with one, two, and three copies of A9g, respectively, compared to HJ alone for $PC3^+$ cells, and 6-, 9-, and 14-fold increase with one, two, and three copies of A9g, respectively, compared to HJ alone for LNCaP cells). In contrast, we saw no appreciable uptake in the PSMA-negative $PC3^-$ cells for any of the three constructs. This result was confirmed by confocal microscopy, where the extent of the Cy5 signal correlated with the number of aptamers attached to the HJ, as shown in Figures 5C and S6. The primarily intracellular signal suggests that A9g-conjugated HJs are internalized (Figure S6). As an additional negative control, we attached a non-binding 46-nt single-stranded DNA oligonucleotide (DNAcont) to the HJ in one to three copies (Figure 3D). HJs carrying up to three copies of DNAcont did not bind significantly better than did naked HJ to any of the cell lines tested (Figures 4B and 5B). This demonstrates that cell uptake is facilitated by the aptamers and is not due to the increased charge of the assembled constructs.

In Vivo Tumor Targeting of HJ-A9g

To investigate whether multimerization of the A9g anti-PSMA aptamer can drive to tumor targeting *in vivo*, we engrafted male nude

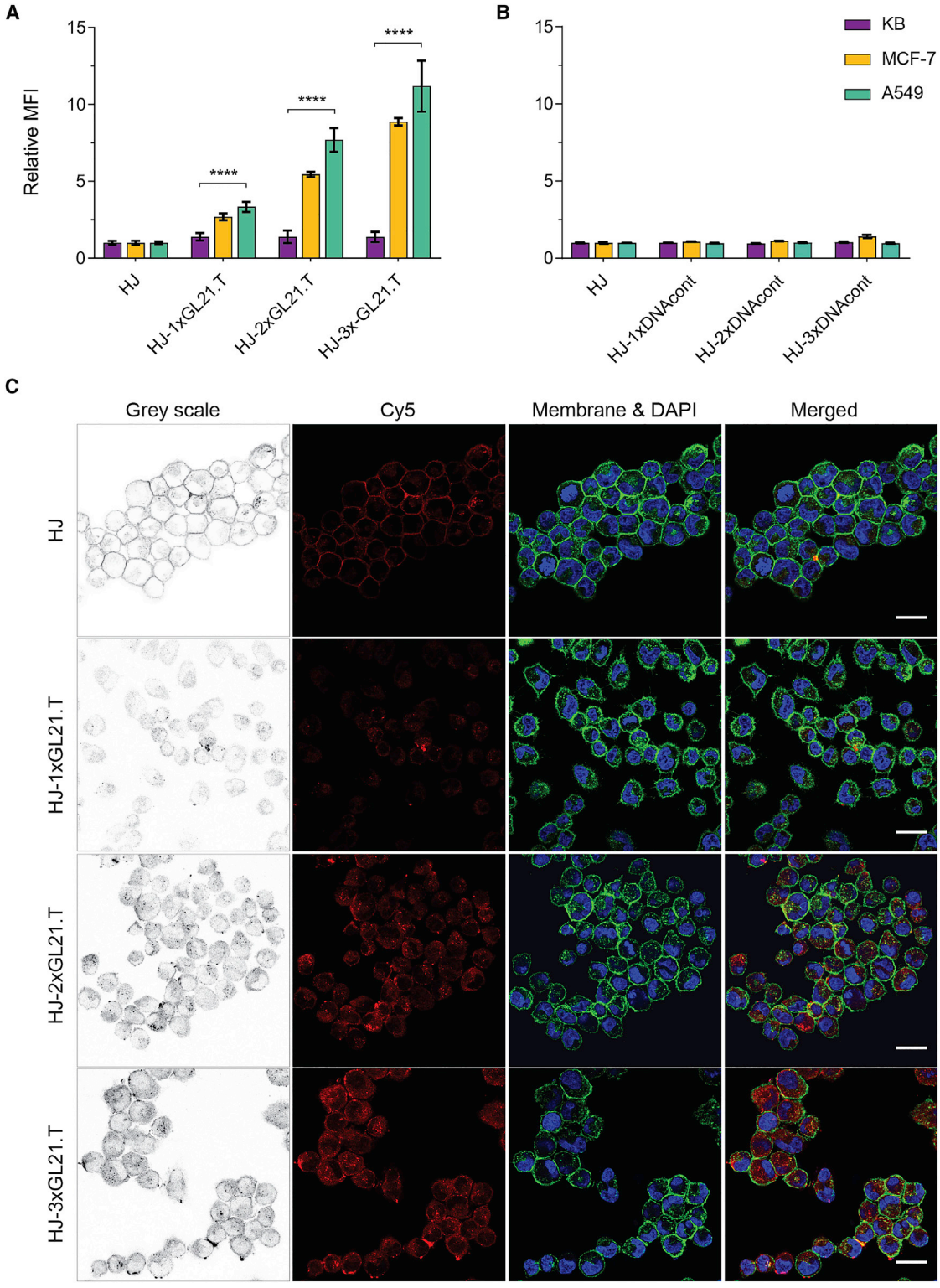

Figure 4. Internalization of Multimeric GL21.T Aptamers

(A) Relative uptake of GL21.T-functionalized HJs in A549, MCF-7, and KB cells analyzed by flow cytometry. The bars represent the quantified MFI from cells treated with three different concentrations (25, 50, or 100 nM) of HJs in three biological replicates, from two independent experiments, normalized to HJ-Cy5. Representative histograms are

(legend continued on next page)

mice with $PC3^+$ (PSMA-positive) and $PC3^-$ (PSMA-negative) cancer cells.

One nanomole of Cy5.5-labeled HJs without or with one, two, or three copies of conjugated A9g aptamers, as well as free Cy5.5-labeled A9g aptamer as a control (Figure 6A), was injected subcutaneously in mice bearing one $PC3^+$ and one $PC3^-$ tumor on each flank. The mice were sacrificed 24 h after injection, and their organs and tumors were scanned *ex vivo* (Figure S7). We observed an approximately 4-fold stronger tumor accumulation with the triple-conjugated HJ in the $PC3^+$-derived tumors compared to $PC3^-$ tumors (Figure 6B), with a trend showing increased $PC3^+$ tumor localization as a function of aptamer copies.

DISCUSSION

The capacity of nucleic acid aptamers to recognize cell surface proteins has enabled their use as targeting ligands for cancer and other disease-related cells. However, to ensure selective binding to a small proportion of cancer cells in the background of the whole body, it may be necessary to multimerize the aptamers to achieve multi-topic recognition of cancer signals. In this study, we demonstrated that a small, stable oligonucleotide structure, the HJ, can be used as a scaffold to multimerize cancer-targeting aptamers and achieve enhanced receptor-mediated targeting of cancer cells *in vitro* and *in vivo*.

Previous studies have used the A10-3 and GL21.T aptamers as targeting agents for siRNAs, based on annealing with an antisense strand.[18,22] We found that a similar approach could be used to attach an aptamer to the multifunctional HJ structure, while maintaining the targeting function of the aptamer. By simple elongation of one *in vitro*-transcribed HJ oligonucleotide with the A10-3 or A9g anti-PSMA aptamers, the system was shown to mediate effective uptake in PSMA-positive cells. However, due to the lack of stabilizing LNA residues in the transcribed RNA, this method could not be extended to multimerized copies of aptamers.

In order to take full advantage of the HJ structure and multimerize aptamers in a truly modular manner, we used a two-step covalent conjugation strategy, in which chemically synthesized aptamers were coupled to HJ oligonucleotides using click chemistry. The advantage of this protocol is that we readily can prepare different HJ structures from the purified arms without the need for further purification. Using two cancer-specific aptamers, that is, AXL receptor-specific GL21.T and PSMA-specific A9g, we successfully self-assembled HJs configured of one, two, and three aptamers as well as a fluorophore for bioimaging purposes. We observed a strong avidity effect in cell binding and internalization upon multimerization for both aptamers. When testing the cell specificity, we found that GL21.T also bound to MCF-7 cells, although this cell line is reported, and confirmed by us, to be AXL negative. These unanticipated results could partially be explained by the fact that the predecessor of GL21.T, namely GL21, was selected using differential whole-cell systematic evolution of ligands by exponential enrichment (SELEX) according to the recently retracted paper by Cerchia et al.[20] In fact, several studies have found inconsistencies in binding affinity and specificity of aptamers that are selected using similar approaches. Another cause of inconsistency has been associated with the means by which selected aptamers are characterized.[23,24] Although negative selection steps are included during cell-SELEX, aptamers with low target specificity are inevitably co-selected due to high target density on the cell surface. In fact, Cerchia et al.[21] disclosed that the GL21.T also binds to the ectodomain of RTK Tyro3 (Sky, Dtk) with a dissociation constant (K_D) of ~43 nM. TYRO3 is an understudied RTK that belongs to the TAM (TYRO3, AXL, MERTK) family of RTK and has an extracellular domain that shares great similarity with that of AXL.[25] Furthermore, the AXL-negative MCF-7 cells have been reported to express TYRO3.[26] We speculate that the AXL-independent binding of GL21.T to MCF-7 cells may be explained by the structural similarity between TYRO3 and AXL and the fact that TYRO3 is highly expressed in MCF-7.

The avidity effect from multimerizing the aptamers observed *in vitro* was less strong *in vivo* where an ~4-fold increased tumor accumulation was observed. This result is in contrast to the strong accumulation of a monovalent A9g in PSMA-positive tumors with no detectable signal for a non-binding aptamer reported by Dassie et al.[16] Certainly, this inconsistency may arise from variations in the experimental setup, particularly when comparing preclinical animal studies.

A multimerized receptor-targeting system for tumors could be highly applicable for improving clinical imaging, e.g., using PSMA-11 positron-emission tomography (PET) tracer,[27,28] or for delivery of drugs and radiochemicals. Many prostate cancer drugs have to be given in a suboptimal dose due to their predominant accumulation in the kidneys, which could lead to renal toxicity.[29] To address these issues, the HJ could be envisioned as a useful theranostic platform for achieving both more sensitive imaging and, at the same time, lower kidney toxicity. Also, by functionalizing the system with both the A9g and the A10-3, it is possible that the different binding and inhibitory properties of these two aptamers could be used to form a multiparatopic, PSMA-specific inhibitory HJ.

MATERIALS AND METHODS

Sequences

The sequences used in this study are as follows: Q1: 5′-NH_2-C6-mC+-CmG+TmCmCmT+GmA+GmCmC-3′; Q2: 5′-NH_2-C6-mCmA+

shown for HJ-A9g constructs in Figure S4. (B) Flow cytometry analysis of HJs carrying one to three copies of non-binding control DNA oligonucleotide (DNAcont) in A549, MCF-7, and KB cells. The bars represent quantified MFI from cells treated with 50 nM HJs in three biological replicates, normalized to HJ-Cy5. For comparison of multiple groups in each cell line, statistical analysis was conducted using two-way ANOVA followed by a Tukey's post hoc test. Error bars represent mean ± SD. ****$p < 0.0001$, for each increase in valency. (C) Confocal microscopy of HJ-GL21.T internalization in A549 cells. Red shows signal from Cy5 coupled HJs, gray shows the Cy5 signal converted on a white background, blue shows DAPI nucleus stain, and green shows WGA-Alexa 488 membrane stain. Orthogonal view of internalized HJ-3xGL21.T is provided in Figure S5. Brightness and contrast are kept constant in all images. Scale bars, 21 μm.

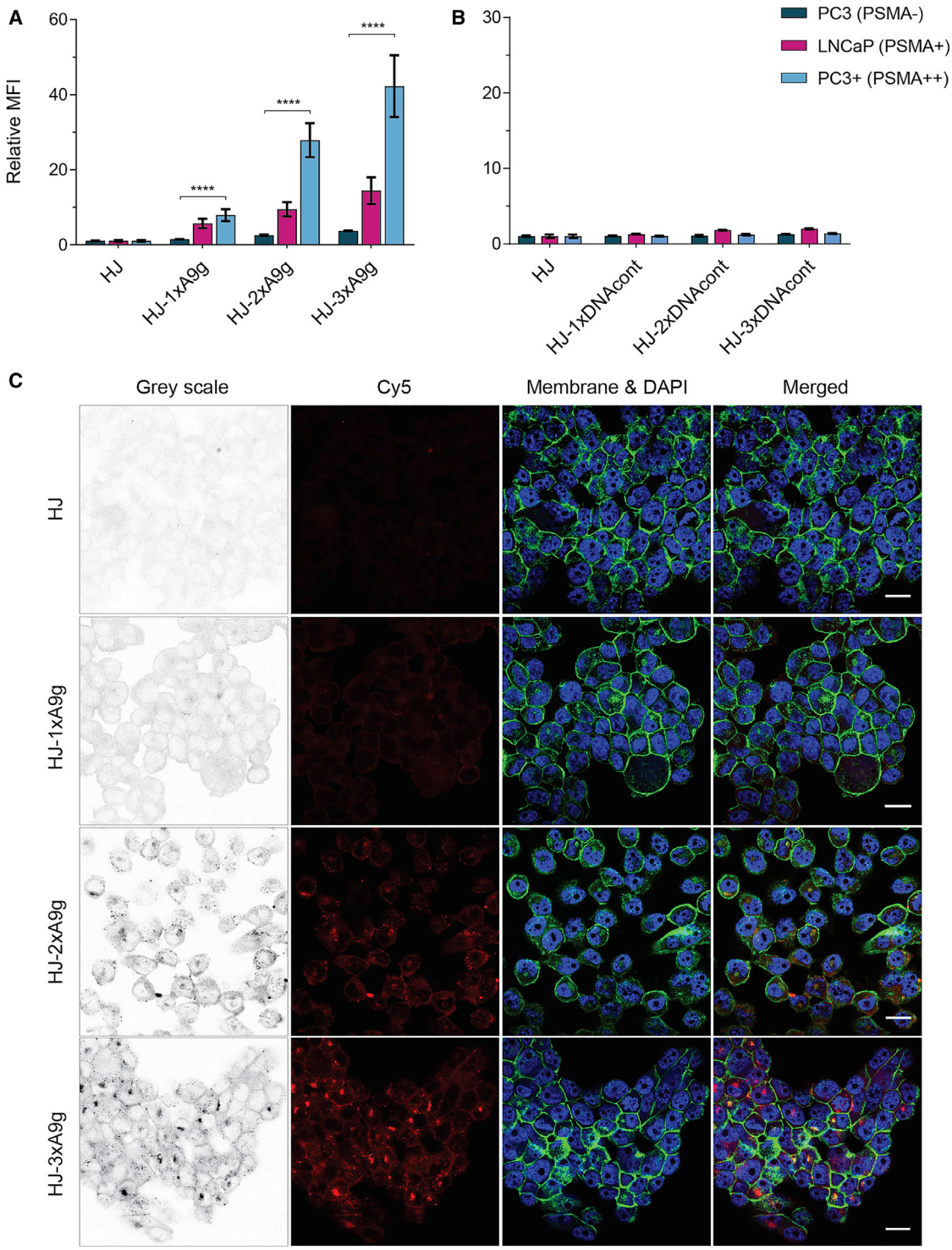

Figure 5. Internalization of Multimeric A9g Aptamers

(A and B) Relative uptake of A9g-functionalized HJs (A) or HJ-DNAcont (B) in PC3^{+} (PSMA^{++}), LNCaP (PSMA^{+}), and PC3 (PSMA^{-}) cells analyzed by flow cytometry. The bars represent the quantified MFI from cells treated with 50 nM of the denoted HJ construct (three biological replicates, from two independent experiments) normalized to HJ-Cy5. Statistics were analyzed by two-way ANOVA followed by Tukey's post hoc test. Error bars represent mean ± SD. ****$p < 0.0001$, for each increase in valency. (C) Confocal microscopy images of HJ-A9g internalization in PC3^{+} cells. Red shows Cy5, gray shows a converted Cy5 signal, blue shows DAPI nucleus stain, and green shows membrane stain. Brightness and contrast are kept constant in all images. Scale bars, 21 μm.

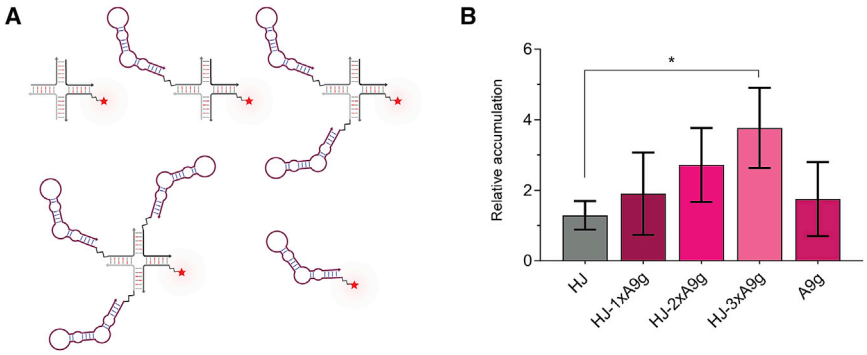

Figure 6. *In Vivo* Tumor Targeting with Multimeric A9g-Conjugated HJ

(A) Schematics of assembled HJ-A9g constructs and free A9g-Cy5.5. (B) Relative tumor accumulation between PSMA-positive and PSMA-negative tumors paired in the same mouse. Statistical analysis was performed using one-way ANOVA followed by a Tukey's post hoc test. Number of mice in each group was at least four. Error bars represent mean ± SD. *$p < 0.05$.

CmA+GmTmG+GmA+CmGmG-3′; Q3: 5′-NH_2-C6-mG+GmC+TmCmAmCmC+GmA+TmC-3′; Q4: 5′-NH_2-C6-mGmA+TmC+GmGmAmC+TmG+TmG-3′; GL21.T: 5′-NH_2-C6-rAfUrGrAfUfCrArAfUfCrGfCfCfUfCrArAfUfUfCrGrAfCrArGrGrArGrGfCfUfCrAfC-3′; A9g: 5′-NH_2-C5-rGrGrGrAfCfCrGrArArArArArGrAfCfCfUrGrAfCfUfUfCfUrAfUrAfCfUrArArGfUfCfUfCrGfUfUfCfCfC-3′; Q3.A10-3 template, forward: 5′- TAGAATTCTAATACGACTCACTATAGGGCTCACCGATCGGGAGGACGATGCGGA-3′; Q3.A10-3 template, reverse: 5′-TTAGGAGTGACGTAAACATGGCTGATCCGCATCGTCCTCCCGATCGGTGAGCCC-3′; Q3.A9g template, forward: 5′-TCTAATACGACTCACTATAGGGCTCACCGATCTTGGGACCGAAAAAGACCTGACTTCTATACTAAGTCTACGTTCCC-3′; Q3.A9g template, reverse: 5′-GGGAACGTAGACTTAGTATAGAAGTCAGGTCTTTTTCGGTCCCAAGATCGGTGAGCCCTATAGTGAGTCGTATTAGA-3′; DNA control: 5′-NH_2-C6-CGACGACGACGACGACGACCCCTCGTCGTCGTCGTCGTCG TCG-3′. LNA nucleotides are denoted with "+," RNA with "r," 2′-F nucleotides with "f", and 2′-OMe with "m." A9g and GL21.T aptamers were purchased from Dharmacon. Q1, Q2, Q3, and Q4 were synthesized by the group of Jesper Wengel (University of Southern Denmark [SDU]), as previously described.[14] All DNA strands were purchased from Sigma-Aldrich.

In Vitro Transcription of Q3.A10-3 and Q3.A9g

For the aptamer construct Q3.A9g, a DNA template was prepared by mixing equimolar amounts of the forward (Q3.A9g template, forward) and reverse (Q3.A9g template, reverse) primer. For the Q3.A10-3 derivative, the forward (Q3.A10-3 template, forward) and reverse (Q3.A10-3 template, reverse) primers were first annealed and then extended with Klenow enzyme as described by the manufacturer (Thermo Scientific). The resulting template DNA was gel-purified before transcription.

Both templates were mixed in T7 buffer (80 mM HEPES [pH 7.5], 2.5 mM NTP mix [ATP, CTP, 2′-F- deoxycytidine triphosphate (dCTP), 2′-F-deoxyuridine triphosphate (dUTP)], 0.1 mg/mL BSA, 20 mM $MgCl_2$, 10 mM DTT, 1 mM spermidine, and 20 μL of pyrophosphatase [50 U/mL]) in a total volume of 200 μL. Transcription was initiated by the addition of Y639F T7 RNA polymerase (purified in-house) and incubated at 37°C overnight (O/N). The transcripts were gel-purified followed by phenol/chloroform extraction and ethanol precipitation. All RNAs were subsequently analyzed on a 12% denaturing PAGE gel.

Conjugation and Assembly of HJ

For detection purpose, the Q2 oligonucleotide was reacted with 100-fold molar excess of *N*-hydroxysuccinimide (NHS)-Cy5 or NHS-Cy5.5. For the synthesis of oligonucleotide-aptamer conjugates, Q1, Q3, and Q4 oligonucleotides were reacted with 50-fold molar excess of NHS-dibenzocyclooctyne (DBCO), while the synthetic aptamers were reacted with 50-fold molar excess of NHS-azide. All reactions with activated NHS esters were carried out in 100 mM HEPES (pH 8.2), 30%–50% DMSO at 25°C, 500 rpm for 4–24 h. All NHS reagents were purchased from Lumiprobe.

Copper-free click reactions between DBCO-labeled Q oligonucleotides and azide-labeled aptamers were carried out in 100 mM HEPES (pH 7.5), 45% DMSO at 30°C, 500 rpm shaking for 4 h. The reactions were carried out in a 1:1.5 ratio of Q oligonucleotide to GL21.T aptamer, to correct for the amount of unreacted aptamer without azide label remaining in solution or with a 2.5-fold excess of Q-DBCO to A9g to allow for better separation in the HPLC purification. All reaction products were analyzed on a 12% denaturing PAGE gel.

Reaction products were purified by RP-HPLC on a Phenomenex Kinetex XB C18 column with a MeCN gradient from 5% MeCN, 5% triethylammonium acetate (TEAA) to 95% MeCN over 25 min, 6 min 95% MeCN, and 7 min 100% MeCN. Conjugates of Q oligonucleotides and the A9g aptamer were purified using 10% TEAA. Fractions containing the products were collected and lyophilized.

HJs were assembled by mixing all four oligonucleotides in equal amounts in a final concentration of 200 mM KOAc for *in vitro* experiments and PBS for *in vivo* use. The samples were heated to 70°C and cooled to 4°C following a linear temperature ramp during 90 min in a thermocycler. All assemblies were analyzed by 12% native PAGE.

Cell Culture

The prostate cancer cell lines $PC3^+$ ($PSMA^+$) and PC3 ($PSMA^-$) were a kind gift from Dr. Paloma Giangrande from the Department of Internal Medicine, University of Iowa, USA. The A549 and

MCF-7 cells were generously provided by Dr. Vittorio de Franciscis from the Institute of Endocrinology and Experimental Oncology, CNR, Napoli, Italy. Both KB and LNCaP cells were purchased from ATCC.

PC3 cells were grown in F12 Kaighn's modification medium (GE Healthcare), KB cells were grown in RPMI 1640 medium (Sigma-Aldrich), LNCaP cells were grown in RPMI 1640 medium (ATTC), A549 cells were grown in RPMI 1640 medium (Gibco), and MCF-7 cells were grown in Eagle's minimal essential medium EMEM (ATCC), all supplemented with 10% fetal bovine serum (FBS) (Gibco) and 1% penicillin/streptomycin (P/S) (full medium), at 37°C, 5% CO_2. For seeding for flow cytometry and confocal microscopy, the cells were washed with Dulbecco's phosphate-buffered saline (PBS) and released by incubation with 0.05% trypsin-EDTA (1×) (Gibco) for 5–10 min. The cells were centrifuged at 200 × *g* for 5 min and resuspended in full medium. Cell number and viability was determined with a Via-1 cassette counting chamber (ChemoMetec), using the software NucleoView NC-200.

Culture flasks, microscopy slides, and 24-well plates for LNCaP cells were coated with 100 μg/mL poly-L-lysine (PLL) (Sigma-Aldrich) in PBS, and incubated at room temperature (RT) for 15 min. The excess PLL was removed by washing three times with PBS, before the addition of cells.

Flow Cytometry

Cells were seeded at 100,000–150,000 cells per well in 24-well plates 1 day prior to analysis. For uptake experiments with *in vitro*-transcribed aptamers, $PC3^-$ and LNCaP cells were treated for 45 min with medium, Cy5-labeled HJ, or HJ-anti-PSMA aptamers (50 nM) before harvesting the cells for flow cytometry. For uptake studies of the covalently conjugated aptamers, A9g and GL21.T, the cells were pre-incubated with 100 μg/mL salmon sperm DNA for 10 min to block unspecific binding. The cells were treated in three replicates with medium, 50 nM Cy5-labeled HJ, or aptamer-functionalized HJs for different periods of time (2 h for GL21.T and 45 min for A9g). For antibody detection of the AXL receptor, cells were pre-incubated for 10 min with 100 μg/mL human immunoglobulin G (IgG) to block unspecific antibody binding, and subsequently incubated with 7 nM AXL mAb-phycoerythrin (PE) (DS7HAXL), or mouse IgG1κ isotype control-PE (eBioscience), for 15 min. After incubation, the cells were washed three times with PBS and trypsinated for 10 min. Cells were resuspended in full medium, transferred to Eppendorf tubes, and centrifuged for 10 min at 2,000 × g. The supernatant was removed, and the cells were again washed with PBS, centrifuged, and resuspended in PBS for analysis.

Flow cytometry of HJ-Q3.A10-3 and HJ-Q3.A9g was done on a Gallios flow cytometer (Beckman Coulter), while analysis of synthetic A9g, GL21.T, and DNAcont was performed on a NovoCyte flow cytometer (ACEA Biosciences) using the NovoExpress software.

Confocal Microscopy

For confocal microscopy, 50,000–100,000 LNCaP cells were seeded on PLL-coated slides, while A549, PC3, and MCF7 cells were seeded on uncoated slides in full medium 1 day prior to treatment. Samples were added to the medium of the cells (medium, Cy5-labeled HJ or HJ-aptamer in 200 nM) and incubated at 37°C for 45 min for A9g and 2 h for GL21.T. The medium was removed, and the cells were washed three times with PBS. The cells were stained with 200 μL of 2.5 μg/mL wheat germ agglutinin (WGA)-Alexa 488 (Thermo Scientific) for 15 min at 37°C. The cells were washed three times with PBS and fixed by adding 200 μL of 4% paraformaldehyde (PFA) and incubated at 37°C for 15 min. Samples were washed with PBS, dried, and stained with one drop of DAPI ProLong Gold (Invitrogen) to each position on the slide. After mounting of the cover slide, the sample was incubated at 4°C O/N. Cells were imaged on a confocal laser scanning microscope (Zeiss LSM 700) with a ×63 oil objective. All images within one experiment were acquired with identical laser and filter settings and subsequently adjusted for brightness and contrast equally in Fiji software for improved visualization.

Animal Experiments

All animal studies were approved by the Animal Experiments Inspectorate, under the Danish Veterinary and Food Administration License no. 2013-15-2934-00901. All animals were provided with standard rodent diet and water. All animals were kept in groups of four to five mice per cage throughout the experiments.

Male athymic nude mice (BALB/c-AnNRj-Foxn1nu) were xenografted by subcutaneous injection of $PC3^+$ and $PC3^-$ cells in the right and left flank, respectively (1×10^6 cells per tumor), dissolved in ice-cold Matrigel (BD Biosciences). Approximately 4 weeks following tumor grafting, HJs were injected intravenously with 200 μL of PBS or 1 nmol of sample resuspended in 200 μL of PBS. Mice were sacrificed 24 h post-injection by cervical dislocation. The tumors and organs were collected and scanned for Cy5.5 fluorescence in an IVIS Spectrum *in vivo* imaging system (Xenogen, Caliper Life Sciences, Hopkinton, MA, USA). Using the software Living Image version 4.3.1 (Caliper Life Sciences), the fluorescent signal was subjected to spectral unmixing by using the system's in-built Cy5.5 filter settings and a mouse control treated with only PBS. Specifically, images were first subjected to spectral unmixing using the organs from a PBS-treated mouse as a negative control. Regions of interest were identified manually before recording the fluorescent signal. In the further analysis, we used the average radiant efficiency.

Statistical Analysis

All statistical analyses were performed in Prism 8 (GraphPad, San Diego, CA, USA). All data are presented as mean ± SD. Statistical analysis for comparing multiple groups in each cell line was analyzed by either one-way or two-way ANOVA with a post hoc Tukey's test. Brackets with asterisks represent statistical differences as follows: *p <0.05, **p <0.01, and ****p <0.0001. The specific statistical method used and the number of replicates are described in the figure legends.

SUPPLEMENTAL INFORMATION

Supplemental Information can be found online at https://doi.org/10.1016/j.omtn.2020.10.013.

AUTHOR CONTRIBUTIONS

M.O., V.L.A., and J.S.N carried out the experiments. V.L.A. drafted the manuscript. J.K., J.W, and J.S.N supervised and designed the experiments. All authors have read and edited the manuscript.

CONFLICTS OF INTEREST

The authors declare no competing interests.

ACKNOWLEDGMENTS

The authors thank Dr. Frederik Dagnæs-Hansen at the Department of Biomedicine, Aarhus University, for help with the animal studies. A big thanks to the Center Manager for Cellular Signal Patterns (CellPAT) Anne F. Nielsen for reading and editing this manuscript. This work was supported by grant DNRF135 from the Danish National Research Foundation to the Center for Cellular Signal Patterns (CellPAT) and, in part, by the Novo Nordisk Foundation to the Center for Multifunction Biomolecular Drug Design (CEMBID) (grant NNF17OC0028070), and by the Villum Foundation to the Center for Biomolecular Nanoscale Engineering (BioNEC) (grant 18333).

REFERENCES

1. Srinivasarao, M., Galliford, C.V., and Low, P.S. (2015). Principles in the design of ligand-targeted cancer therapeutics and imaging agents. Nat. Rev. Drug Discov. *14*, 203–219.
2. Tuerk, C., and Gold, L. (1990). Systematic evolution of ligands by exponential enrichment: RNA ligands to bacteriophage T4 DNA polymerase. Science *249*, 505–510.
3. Nimjee, S.M., White, R.R., Becker, R.C., and Sullenger, B.A. (2017). Aptamers as therapeutics. Annu. Rev. Pharmacol. Toxicol. *57*, 61–79.
4. Kaur, H., Bruno, J.G., Kumar, A., and Sharma, T.K. (2018). Aptamers in the therapeutics and diagnostics pipelines. Theranostics *8*, 4016–4032.
5. Silver, D.A., Pellicer, I., Fair, W.R., Heston, W.D., and Cordon-Cardo, C. (1997). Prostate-specific membrane antigen expression in normal and malignant human tissues. Clin. Cancer Res. *3*, 81–85.
6. McNamara, J.O., Kolonias, D., Pastor, F., Mittler, R.S., Chen, L., Giangrande, P.H., Sullenger, B., and Gilboa, E. (2008). Multivalent 4-1BB binding aptamers costimulate $CD8^+$ T cells and inhibit tumor growth in mice. J. Clin. Invest. *118*, 376–386.
7. Pratico, E.D., Sullenger, B.A., and Nair, S.K. (2013). Identification and characterization of an agonistic aptamer against the T cell costimulatory receptor, OX40. Nucleic Acid Ther. *23*, 35–43.
8. Chu, T.C., Twu, K.Y., Ellington, A.D., and Levy, M. (2006). Aptamer mediated siRNA delivery. Nucleic Acids Res. *34*, e73.
9. Breitz, H.B., Weiden, P.L., Beaumier, P.L., Axworthy, D.B., Seiler, C., Su, F.M., Graves, S., Bryan, K., and Reno, J.M. (2000). Clinical optimization of pretargeted radioimmunotherapy with antibody-streptavidin conjugate and 90Y-DOTA-biotin. J. Nucl. Med. *41*, 131–140.
10. Krissanaprasit, A., Key, C., Fergione, M., Froehlich, K., Pontula, S., Hart, M., Carriel, P., Kjems, J., Andersen, E.S., and LaBean, T.H. (2019). Genetically encoded, functional single-strand RNA origami: anticoagulant. Adv. Mater. *31*, e1808262.
11. Okholm, A.H., and Kjems, J. (2016). DNA nanovehicles and the biological barriers. Adv. Drug Deliv. Rev. *106* (Pt A), 183–191.
12. Farokhzad, O.C., Jon, S., Khademhosseini, A., Tran, T.-N.T., LaVan, D.A., and Langer, R. (2004). Nanoparticle-aptamer bioconjugates. Cancer Res. *64*, 7668–7672.
13. Sun, T., Zhang, Y.S., Pang, B., Hyun, D.C., Yang, M., and Xia, Y. (2014). Engineered nanoparticles for drug delivery in cancer therapy. Angew. Chem. Int. Ed. Engl. *53*, 12320–12364.
14. Andersen, V.L., Vinther, M., Kumar, R., Ries, A., Wengel, J., Nielsen, J.S., and Kjems, J. (2019). A self-assembled, modular nucleic acid-based nanoscaffold for multivalent theranostic medicine. Theranostics *9*, 2662–2677.
15. Rockey, W.M., Hernandez, F.J., Huang, S.-Y., Cao, S., Howell, C.A., Thomas, G.S., Liu, X.Y., Lapteva, N., Spencer, D.M., McNamara, J.O., et al. (2011). Rational truncation of an RNA aptamer to prostate-specific membrane antigen using computational structural modeling. Nucleic Acid Ther. *21*, 299–314.
16. Dassie, J.P., Hernandez, L.I., Thomas, G.S., Long, M.E., Rockey, W.M., Howell, C.A., Chen, Y., Hernandez, F.J., Liu, X.Y., Wilson, M.E., et al. (2014). Targeted inhibition of prostate cancer metastases with an RNA aptamer to prostate-specific membrane antigen. Mol. Ther. *22*, 1910–1922.
17. Lupold, S.E., Hicke, B.J., Lin, Y., and Coffey, D.S. (2002). Identification and characterization of nuclease-stabilized RNA molecules that bind human prostate cancer cells via the prostate-specific membrane antigen. Cancer Res. *62*, 4029–4033.
18. McNamara, J.O., 2nd, Andrechek, E.R., Wang, Y., Viles, K.D., Rempel, R.E., Gilboa, E., Sullenger, B.A., and Giangrande, P.H. (2006). Cell type-specific delivery of siRNAs with aptamer-siRNA chimeras. Nat. Biotechnol. *24*, 1005–1015.
19. Dassie, J.P., Liu, X.Y., Thomas, G.S., Whitaker, R.M., Thiel, K.W., Stockdale, K.R., Meyerholz, D.K., McCaffrey, A.P., McNamara, J.O., 2nd, and Giangrande, P.H. (2009). Systemic administration of optimized aptamer-siRNA chimeras promotes regression of PSMA-expressing tumors. Nat. Biotechnol. *27*, 839–849.
20. Cerchia, L., Esposito, C.L., Jacobs, A.H., Tavitian, B., and de Franciscis, V. (2020). Retracted. PLoS ONE *15*, e0228838.
21. Cerchia, L., Esposito, C.L., Camorani, S., Rienzo, A., Stasio, L., Insabato, L., Affuso, A., and de Franciscis, V. (2012). Targeting Axl with an high-affinity inhibitory aptamer. Mol. Ther. *20*, 2291–2303.
22. Esposito, C.L., Cerchia, L., Catuogno, S., De Vita, G., Dassie, J.P., Santamaria, G., Swiderski, P., Condorelli, G., Giangrande, P.H., and de Franciscis, V. (2014). Multifunctional aptamer-miRNA conjugates for targeted cancer therapy. Mol. Ther. *22*, 1151–1163.
23. Cibiel, A., Quang, N.N., Gombert, K., Thézé, B., Garofalakis, A., and Ducongé, F. (2014). From ugly duckling to swan: unexpected identification from cell-SELEX of an anti-annexin A2 aptamer targeting tumors. PLoS ONE *9*, e87002.
24. Civit, L., Taghdisi, S.M., Jonczyk, A., Haßel, S.K., Gröber, C., Blank, M., Stunden, H.J., Beyer, M., Schultze, J., Latz, E., and Mayer, G. (2018). Systematic evaluation of cell-SELEX enriched aptamers binding to breast cancer cells. Biochimie *145*, 53–62.
25. Linger, R.M.A., Keating, A.K., Earp, H.S., and Graham, D.K. (2008). TAM receptor tyrosine kinases: biologic functions, signaling, and potential therapeutic targeting in human cancer. Adv. Cancer Res. *100*, 35–83.
26. Ekyalongo, R.C., Mukohara, T., Kataoka, Y., Funakoshi, Y., Tomioka, H., Kiyota, N., Fujiwara, Y., and Minami, H. (2013). Mechanisms of acquired resistance to insulin-like growth factor 1 receptor inhibitor in MCF-7 breast cancer cell line. Invest. New Drugs *31*, 293–303.
27. Schäfer, M., Bauder-Wüst, U., Leotta, K., Zoller, F., Mier, W., Haberkorn, U., Eisenhut, M., and Eder, M. (2012). A dimerized urea-based inhibitor of the prostate-specific membrane antigen for 68Ga-PET imaging of prostate cancer. EJNMMI Res. *2*, 23.
28. Eder, M., Schäfer, M., Bauder-Wüst, U., Hull, W.-E., Wängler, C., Mier, W., Haberkorn, U., and Eisenhut, M. (2012). 68Ga-complex lipophilicity and the targeting property of a urea-based PSMA inhibitor for PET imaging. Bioconjug. Chem. *23*, 688–697.
29. Yordanova, A., Eppard, E., Kürpig, S., Bundschuh, R.A., Schönberger, S., Gonzalez-Carmona, M., Feldmann, G., Ahmadzadehfar, H., and Essler, M. (2017). Theranostics in nuclear medicine practice. OncoTargets Ther. *10*, 4821–4828.